ELSEVIER

Journal of Nuclear Materials 244 (1997) 219–226

journal of nuclear materials

The effect of solutes on defect distributions and hardening in ion-irradiated model ferritic alloys

Philip M. Rice *, Roger E. Stoller

Metals and Ceramics Division, Oak Ridge National Laboratory, P.O. Box 2008, Oak Ridge, TN 37831-6376, USA

Received 5 September 1996; accepted 30 October 1996

Abstract

A series of nine model ferritic alloys were ion irradiated at ~300°C using 2.5 MeV He ions to a dose of 1.4×10^{21} ion/m^2, which corresponds to ~0.1 dpa at a depth of 2 μm and ~3.5 dpa at the peak damage region which occurs at about 4 μm deep. The resultant changes in hardness as a function of depth were measured using a Nanoindenter®. TEM was used to investigate the defect distributions. The effect of various solutes, Cu and N in particular, but Mn and Ti as well, on the change of hardness and the defect distribution due to the ion irradiation are discussed.

1. Introduction

Embrittlement of light water reactor (LWR) pressure vessels depends on alloy composition in a complex manner making reliable estimates of their lifetimes difficult to determine [1]. To gain insights into the effect of different solutes on embrittlement, a series of model ferritic alloys with varying solute contents were chosen and characterized. Defects were introduced by ion irradiation. The specimens were then prepared in cross-section to allow microstructural and mechanical property changes to be studied as a function of depth below the irradiated surface. The general technique of using transmission electron microscopy (TEM) to study the microstructural properties and nanoindentation to study the mechanical properties of the ion-irradiated alloys has been reported previously for specimens irradiated with Fe ions [2]. This paper reports the results obtained from irradiations with He ions.

2. Experimental

2.1. Irradiation

A series of high-purity Fe-based model ferritic alloys containing Cu, N, Mn and/or Ti additions, alone or in combination, was used in this investigation. The alloy designations and their compositions are summarized in Table 1. The alloys were obtained from the University of California, Santa Barbara, where they are being used in a series of neutron irradiation experiments [3]. The specimens were irradiated in the as-received condition: solution treated at 775°C for 17 h, quenched in a salt bath to 450°C and held for 3 min and subsequently air cooled. The quenching treatment was intended to maintain a copper supersaturation and the short temper was intended to permit carbide precipitation in the carbon containing alloys. The specimens were irradiated as TEM discs in the ORNL triple ion facility using 2.5 MeV He ions to a dose of 1.4×10^{21} ion/m^2 at a temperature of ~300°C. The accelerator is capable of irradiating nine TEM discs at a time. Each target included three discs of three different alloys. The first target held three discs of each of the alloys 348, 390 and 399. The second target held three discs each of alloys 349, 360 and 373. The third target held three discs each of the alloys 350, 397 and 387. The targets were first heated to approximately 150°C and then the ion beam, at a current of ~0.6 μA/cm^2, was used to heat the specimens to ~300°C. The temperature of the specimens was measured with a thermocouple spot-welded to the front of one of the target specimens. Each target was irradiated for a total of ~11 h over two days.

The TRIM code (versions 91.14 and 92.04) [4] was used to compute the required ion fluences and the displace-

* Corresponding author. Tel.: +1-423 574 2480; fax: +1-423 574 0641; e-mail: ricepm@ornl.gov.

PII S0022-3115(96)00753-2

Table 1
List of alloys and their compositions

Alloy No.	N (appm)	Composition (wt%) (balance Fe)			
		Cu	Mn	C	Ti
VM 348	5	—	—	—	—
VM 349	80	—	—	—	—
VM 350	120	—	—	—	—
VM 360	10	0.89	1.03	< 0.003	—
VM 373	100	< 0.01	0.01	< 0.003	0.3
VM 387	10	0.51	0.05	0.17	0.003
VM 390	20	0.51	0.06	< 0.005	0.002
VM 397	20	0.91	< 0.01	< 0.01	< 0.01
VM 399	120	0.51	0.01	< 0.01	< 0.01

ment dose as a function of depth beneath the specimen surface. The results from TRIM calculations for the specified irradiation conditions are shown in Fig. 1. The solid line goes with the left axis and shows the damage in dpa (displacements per atom) as a function of depth in the specimen. At 2 μm depth the dose is ~ 0.1 dpa; the peak dose of ~ 3.5 dpa occurs just beyond 4 μm. The dashed line goes with the right axis and shows the implanted He concentration [He] in appm (atomic parts per million) as a function of depth. At the 2 μm position [He] = 10 appm, with the peak occurring at 60,000 appm (6 at%) just beyond 4 μm. Thus, both dose and helium content are varying. The region around 2 μm depth has a [He]/dpa = 100 which is of interest for those studying a spallation neutron environment. The dose variations discussed below correspond to measurements made at different depths.

The depth dependent displacement rate in these irradiations varied from 2 to 20×10^{-6} dpa/s over the range of depths examined. This is about 5 orders of magnitude higher than that experienced by a typical reactor pressure vessel (RPV). Thus, this experiment should not be seen as an attempt to simulate RPV in-service conditions. For example, it is well known that accelerated displacement rates can lead to an effective temperature shift in some radiation-induced phenomena [5]. An initial comparison of results obtained at 300 and 400°C indicated that the difference in hardening was not significant for these two temperatures. However, a decision was made to conduct the subsequent irradiations at 300°C to help retain the fine-scale microstructure characteristic of the 280–300°C RPV service temperature.

2.2. Hardness measurements

The technique developed to prepare cross section specimens from ion irradiated discs has been described in detail in a previous paper and so will not discussed here [2]. The change in hardness caused by the irradiation was measured as a function of depth (i.e., distance below the irradiated surface) by using a low load hardness measuring device called the Nanoindenter® [6]. The actual method used for these experiments has also been described previously [2]. Briefly, a row of approximately 100 indents is made at a very shallow angle to the original irradiated surface, starting a few microns beyond the irradiated region and ending in the electroplated layer of Fe at the specimen surface, as shown in Fig. 2(a). Fig. 2(a) is an SEM image of a typical row of indents in one of the model alloys showing the large grained alloy on top and the fine-grained electroplate on the bottom. The dark band which the indents cross marks the end of range of the He ions and is visible due to grooving (i.e., preferential polishing during the electrochemical polishing process) caused by the high concentration of He bubbles in the region. The broken white line is the oxide that grew on the original irradiated surface. Fig. 2(b) is a higher magnification SEM image of the same set of indents as they cross the original irradiated surface and enter the electroplate. Images like this one were used to measure the indent's position with respect to the original irradiated surface, which will be referred to as the 'depth' in the remainder of the paper.

Fig. 3 shows a set of hardness measurements from the Cu-free, low-N alloy 348 taken with indents having contact depths of ~ 50 nm. The indents were done at this contact depth to ensure that a constant and reasonable volume of material was sampled. The hardness measured from indents beyond the irradiated region (> 5 μm) were averaged (shown as the horizontal line) and the change in hardness, ΔH, was measured with respect to this value. The scatter in the hardness measured beyond the implanted zone (i.e., > 5 μm) is representative of the uncertainty in the values measured in the implanted zone. Note that the values at the peak (shown as open circles) are not reliable due to the grooving that occurred in the region. The grooving resulted in the surface not being flat; the area functions of the diamond indenter used to determine the hardness thus have large and unknown errors resulting in

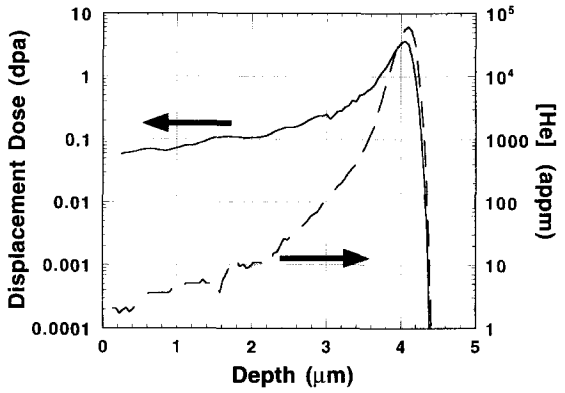

Fig. 1. Displacement dose and the He concentration from TRIM calculations as function of depth in an Fe specimen irradiated with 2.5 MeV He ions.

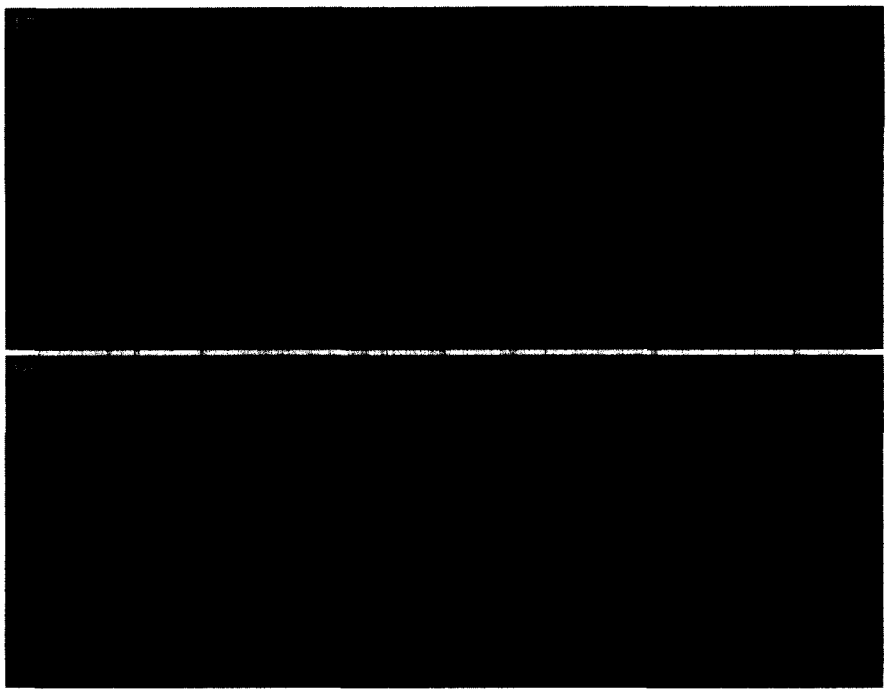

Fig. 2. SEM images of a typical indentation run on one of the model alloys. (a) Low magnification view showing the entire indent run from beyond the irradiated region on the left into the electroplating on the right. (b) Higher magnification image of the indents at the end of the run. (The indents are ~ 100 nm deep, twice that used to acquire the change in hardness data.)

unacceptably large uncertainties in the hardness values taken within ± 0.25 μm of the peak. Measurements similar to those shown in Fig. 3 were made for each of the irradiated alloys and are the basis for the ΔH measurements reported later in the paper (see Figs. 5 and 6).

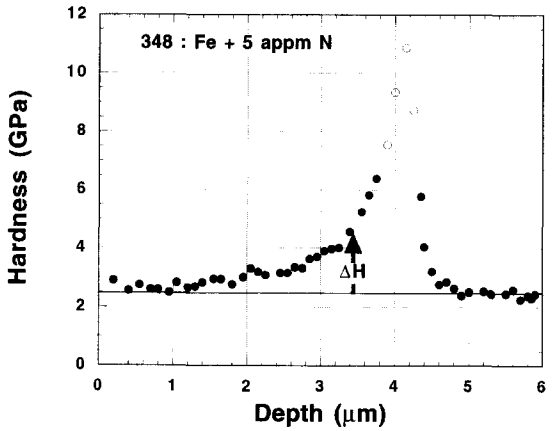

Fig. 3. Hardness values as a function of depth below the originally irradiated surface of alloy 348 using indents with ~ 50 nm contact depths. Values acquired within the grooved portion are marked with open circles since they have large but unknown errors.

2.3. TEM imaging

The cross-sectional specimens were ground to approximately 100 μm thickness and then electrochemically polished to perforation with a twin jet polisher using a perchloric-acid-based electrolyte cooled to -60°C. All TEM imaging was done with a 300 kV Philips CM30 microscope, using $g = \{330\}$ imaging conditions so that the background intensity was weak and the dislocation loops appeared as sharp black spots.

3. Results and discussion

3.1. Hardness measurements

The alloys selected for this set of ion irradiation experiments allowed a broad range of solute effects to be investigated. Fig. 4 is a plot of the change in hardness, ΔH, as a function of wt% Cu for the low-N alloys at various doses. The solid data points are from the He irradiated specimens while the open points represent data from the earlier Fe irradiation [2]. At a dose of 0.07 dpa the Cu-free alloy shows the least hardening due to the delay (threshold) in the onset of hardening (see below), while at 0.20 dpa it shows the greatest change, due to He bubble formation. At the middle dose of 0.1 dpa the relationship appears as

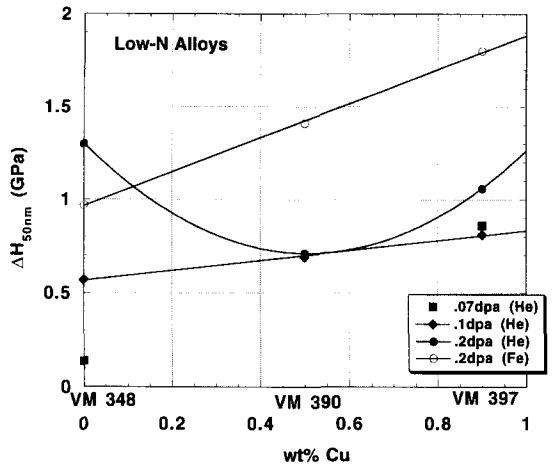

Fig. 4. Measured change in hardness as a function of the weight percent copper at three doses for low nitrogen alloys. The solid points represent data from the He irradiation while the open data points represent earlier data from the Fe irradiation.

linear, perhaps fortuitously. The Cu-free alloy shows no tendency to saturate in this dose range while the Cu-containing alloys clearly show saturation. The change in hardness measured for the Cu-containing alloys irradiated with Fe ions are almost double those observed for He irradiation to similar doses.

The most significant result of the hardness measurements can be seen by separating the alloys into two categories, Cu-free alloys and Cu-containing alloys. A plot of the change in hardness as a function of dose for the Cu-free alloys is displayed in Fig. 5. The indent contact depths were ~ 50 nm and each point on the graph represents the average of four or five measurements made within 0.25 μm of the specific depths 1, 2 and 3 μm. The points at the dose of 0.5 dpa were found by averaging only a few points very near to 3.5 μm, which seems reasonable since the change in hardness appeared to be linear in that region. As a result, the uncertainty in the x direction for these high dose points is larger than for the other points in the figures. The values at the end of range (~ 4.1 μm) of the He ions are not shown here due to their large, unknown errors.

A single nearly linear line has been drawn in Fig. 5 representing the average change of hardening for the Fe–N binary alloys because of the large scatter which seemed independent of the nitrogen content. One of the possible reasons for the weakness of the observed effect is the fact that a significant portion of the nitrogen was observed to have precipitated out in all the high-N alloys in the as-received condition with the exception of the titanium-containing alloy, 373, as reported earlier [7]. However, the effect observed here in the He irradiated samples was that the addition of nitrogen had little or no effect on the hardening which is in contrast to the effect observed for the Fe irradiated samples in which the addition of nitrogen reduced the change in hardness.

When the data are plotted as a function of the square root of dose, and a linear fit to the points is plotted, the above alloys all show a threshold, or a delay in the onset of the hardening. This is in marked contrast to the Cu-containing alloys for which the change of hardness is shown in Fig. 6. For the Cu-containing alloys there is a rapid hardening with low dose. When the data for these alloys are plotted as a function of the square root of dose, a linear fit of the data extrapolated back to zero dose show a common positive ordinate intercept for all the Cu-containing alloys with no indication of a threshold dose. The point

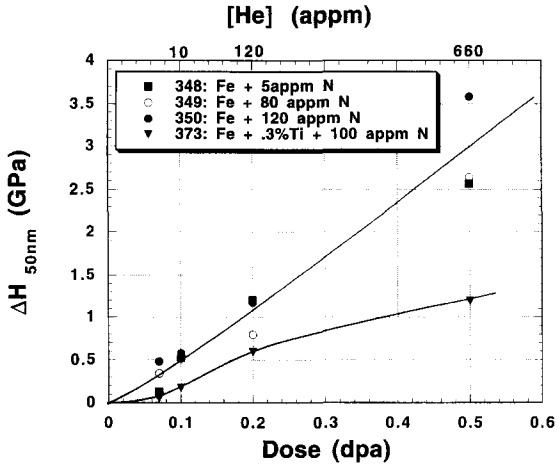

Fig. 5. Change in hardness as a function of the dose for the copper-free alloys. The top line represent the average of the Fe–N binary alloys, while the bottom line is for the Ti-containing alloy 373.

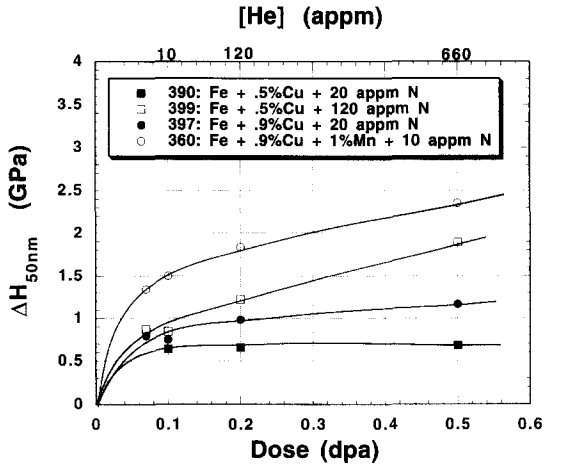

Fig. 6. Change in hardness as a function of the dose for the copper-containing alloys. All alloys show a similar supralinear onset of hardening followed by composition dependent levels of saturation.

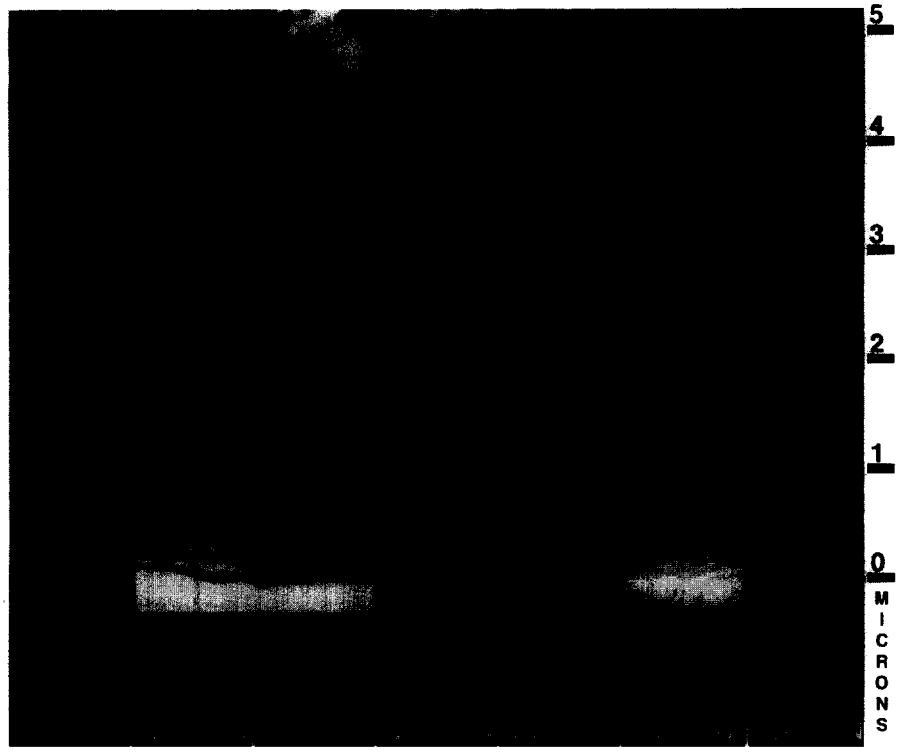

Fig. 7. A survey of the low magnification cross-sectional TEM micrographs showing the entire irradiated region of the major alloys. The scale is on the left and the alloy contents are listed below each image. Note that alloys 390 and 397 show no obvious irradiation damage even at the end of range of the He ions.

at 0.07 dpa for alloy 390 is not shown in Fig. 6 due to the unfortunate circumstance that the hardness values measured in that alloy for the region with that dose were interfered with by a grain boundary running nearly parallel to the irradiated surface.

Comparing alloys 390 and 397 shows that an increase in copper increases the change in hardness at all doses. However, of potentially greater interest is the fact that the two low-nitrogen, Cu-containing alloys 390 and 397 seemed to be unaffected by the high He concentrations. The change in hardness for both alloys remained linear even out to the peak dose/end of range ([He] = 60,000 appm) and neither alloy showed any tendency to groove when polished.

The effect of adding a higher nitrogen concentration to the 0.5% Cu alloy can be seen by comparing alloys 390 and 399. The high nitrogen alloy showed a slightly increased ΔH in the low He region (i.e., ≤ 2.5 μm), but a very large ΔH in the high He region, with the groove forming at the end of range during the polishing procedure.

Comparing alloys 360 with 397 shows that the addition of 1 wt% Mn to the Fe matrix, in conjunction with the 0.9% Cu, doubles the change in hardness due to the irradiation at all doses. The 360 alloy was also observed to groove at the end of range during the polishing process.

3.2. TEM results

3.2.1. Dislocation loop formation

The defect microstructure in each of the irradiated alloys was investigated in cross section using conventional TEM imaging techniques. Fig. 7 shows a survey of the cross-sectional, low magnification micrographs of the irradiated region for most of the alloys. The alloy numbers and their compositions are listed at the base of each micrograph and the depth scale is shown on the right-hand side of the figure. Alloy 349 is not included since it is so similar to alloy 350. All the alloys that showed grooving when polished for nanoindentation show an extremely high defect density at the end of range of the He ions, at and beyond 4 μm. The two low-N, Cu-containing alloys, 390 and 397, show no such peak damage region.

Higher magnification micrographs of the defect structures at the 2 μm depth region (i.e., 0.1 dpa and [He] = 10 appm) are shown in Figs. 8 and 9. The scale marker found in the upper left quadrants apply to all the images in the figures. Note that as yet the thicknesses of the imaged specimen regions have not been determined and thus the reader is cautioned against drawing any conclusions about the density of the defects shown in the figures, but may look at defect sizes only. Comparing alloys 348 and 350

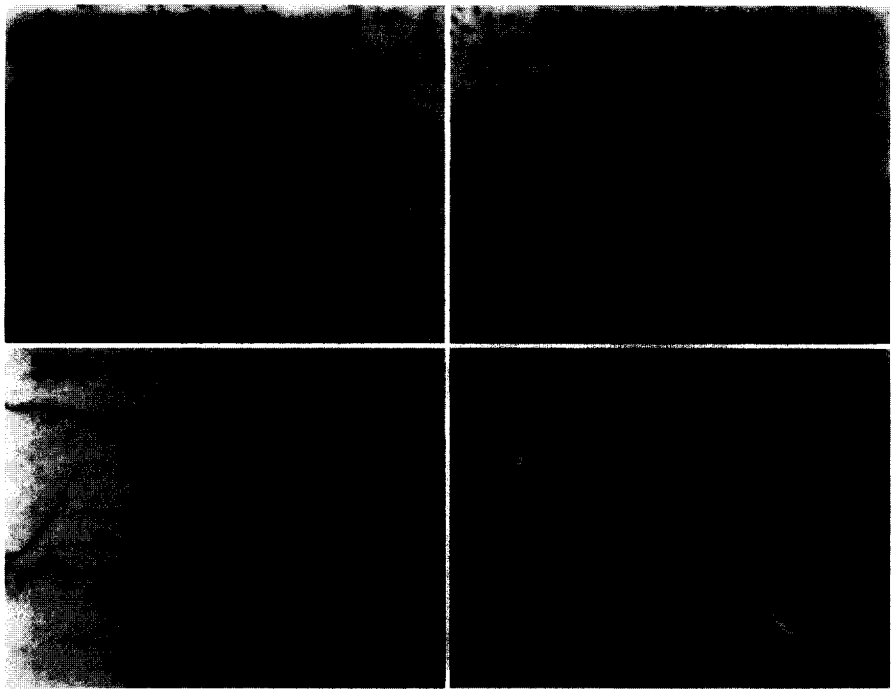

Fig. 8. TEM micrographs of several of the alloys taken at approximately 2 μm depth (0.1 dpa). Comparing left-to-right shows the effect of nitrogen on the defect distribution. Comparing top-to-bottom shows the effect of 0.5% copper on the defect distribution.

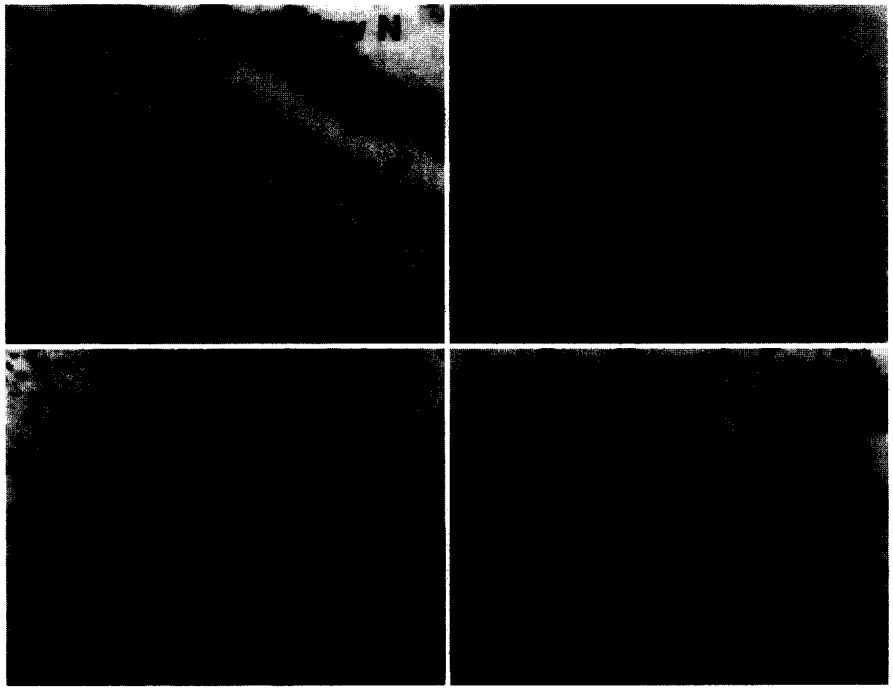

Fig. 9. TEM micrographs of several of the alloys taken at approximately 2 μm depth (0.1 dpa). Comparing left-to-right shows the effect of Mn (top row) and Ti (bottom row) on the defect distribution.

shows that the increase in nitrogen content seems to have slightly decreased the average size of the dislocation loops from $d_{348} \sim 10$ nm to $d_{350} \sim 8$ nm. Comparing alloys 390 and 397 with 348 shows that the addition of Cu (while maintaining low N) seems to have resulted in a complete lack of visible defects being formed (i.e., dislocation loops,

if present, must be less than 2 nm in diameter). A comparison of alloy 399 with 390 shows that when sufficient nitrogen is added to the FeCu alloy, irradiation causes dislocation loops large enough to be visible ($d > 2$ nm) to form.

A comparison of alloy 360 with 397 shows that the addition of Mn to the matrix also results in visible dislocation loops. Although they are just barely visible ($d \leq 2$ nm) there is definitely a higher density of them than in any of the other alloys. This high density of very small dislocation loops correlates well with alloy 360 showing the greatest change in hardness in the low dose, relatively low He region (≤ 2.5 μm).

A comparison of alloy 373 with 350 shows that the addition of 0.3% Ti to the matrix resulted in a suppression of dislocation loop formation but apparently led to precipitation in the irradiated zone. This result is interesting since alloy 373 was the only high-N alloy to retain nitrogen in solution in the as received state, and it showed the least hardening of all the alloys in the low dose, relatively low He region (≤ 2.5 μm). An attempt will be made to identify the apparent precipitates.

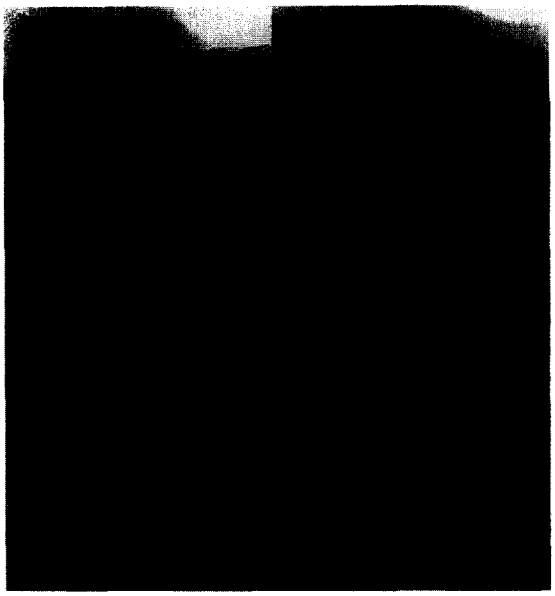

Fig. 10. TEM micrographs of the He bubble formation in alloy 348 due to a dose of 0.5 dpa and a He concentration of 660 appm.

3.2.2. He bubbles

All the alloys with the exception of the low-N, Cu-containing 390 and 397, show extensive He bubble formation in the region beyond 3.75 μm (i.e., [He] $\geq$ 3000 appm). All the bubbles showed a tight size distribution centered at $d \sim 2$ nm. Even at the highest He concentration of $\sim$ 60,000 appm, the bubble density increased but the size of the bubbles remained similar. A close investigation of the He bubbles as a function of depth in the 348 (Fe + low-N) alloy revealed that while there were a few bubbles formed at 2 μm ([He] = 10 appm) significant formation did not occur until beyond 3 μm ([He] = 120 appm). Fig. 10 shows the He bubbles in the 348 alloy at a depth of 3.5 μm (dose = 0.5 dpa and [He] = 660 appm) using Fresnel fringe contrast. In the underfocused condition the bubbles appear as bright in the center with a dark outer fringe, while in the overfocused condition they appear dark with a bright outer fringe.

It is of significant interest that alloys 390 and 397 showed no bubble formation even at the end of range where [He] = 60,000 appm. Since these two alloys were irradiated in separate targets, but with other alloys (390 with 348 and 399, and 397 with 350 and 387) it is clear that the apparent absence of bubbles is due to the effect of chemical composition, not to differences in irradiation conditions. Both alloys showed an increase in hardness as a function of depth and no tendency to groove. To demonstrate that the helium is present a post irradiation anneal was performed on a 397 specimen at 600°C for 24 h and it resulted in extensive bubble/void formation at the end of range depth. Evidently, copper diminishes the availability of vacancies during irradiation. This surprisingly strong Cu-vacancy interaction is consistent with a postulated high copper-vacancy binding energy but may be much greater in a clean Fe–Cu binary alloy [8–10]. This ability of the copper to suppress He bubble formation appears to be negated by either the addition of a substitutional solute like Mn (see alloy 360), or an interstitial solute like N (see alloy 399).

4. Conclusions

A He-ion irradiation study has been carried out on a series of Fe-based alloys containing Cu, N, Mn and/or Ti additions to study the effects of solutes in LWR pressure vessel steels. The following are the principal conclusions.

(1) The experimental technique developed to correlate changes in hardness with changes in the defect microstructure has proved successful.

(2) The Cu-free alloys show a delayed onset of hardening with dose while the Cu-containing alloys all showed a rapid (supralinear) increase in hardening with the initial dose.

(3) The Cu-containing, low-N alloys 390 and 397, which developed no observable defects (i.e., no defects ≥ 2 nm) showed greater hardening in the low He region (< 2.5 μm) and significantly less hardening in the high He region (> 2.5 μm), than the corresponding regions in the Cu-free alloys. This result suggests that the Cu-vacancy interaction is much stronger than previously expected. Manganese seems to reduce this interaction.

(4) Nitrogen is important for encouragement of loops and bubbles. Its effects are diminished by copper.

Acknowledgements

The authors would like to thank Professor G.R. Odette and Professor G.E. Lucas at UCSB for supplying the alloys used in this study. This research was performed at the ORNL SHaRE User Facility and was sponsored by the Division of Materials Sciences, US Department of Energy and the Office of Nuclear Regulatory Research, US Nuclear Regulatory Commission under interagency agreement DOE 1886-8109-8L with the US Department of Energy under contract DE-AC05-960R22464 with Lockheed Martin Energy Research Corp., and by an appointment of PMR to the ORNL Postdoctoral Research Associates Program administered jointly by ORNL and Oak Ridge Institute for Science and Education.

References

[1] G.R. Odette and G.E. Lucas, in: Radiation Embrittlement of Nuclear Reactor Pressure Vessel Steels: An International Review, Vol. 2, ASTM STP 909, ed. L.E. Steels (ASTM, Philadelphia, PA, 1986) p. 206.

[2] P.M. Rice, R.E. Stoller, B.N. Lucas and W.C. Oliver, in: Microstructures of Irradiated Materials, Mater. Res. Soc. Proc., Vol. 373, eds. I.M. Robertson, L.E. Rehn, S.J. Zinkle and W.J. Phythian (MRS, Boston, MA, 1995) p. 149.

[3] G.R. Odette et al., in: Effects of Radiation on Materials: 17th Int. Symp. ASTM STP 1271, eds. D.S. Gelles, R.K. Nanstad, A.S. Kumar and E.A. Little (ASTM, Philadelphia, PA, 1995) p. 547.

[4] J.P. Biersack and L.G. Haggmark, Nucl. Instr. Methods 174 (1980) 257.

[5] L.K. Mansur, Nucl. Techol. 40 (1978) 5.

[6] W.C. Oliver and G.M. Pharr, J. Mater. Res. 7(6) (1992) 1564.

[7] P.M. Rice and R.E. Stoller, Microstructural Characterization of Selected AEA/UCSB Model FeCuMn Alloys, Martin Marietta Energy Systems Inc., Oak Ridge National Laboratory, NUREG/CR-6332 (ORNL/TM-12980) (1996).

[8] G. Salje and M. Feller-Kniepmeier, J. Appl. Phys. 48(5) (1977) 1833.

[9] G.R. Odette and C.K. Sheeks, in: Phase Stability During Irradiation, eds. J.R. Holland, L.K. Mansur and D.I. Potter (The Metallurgical Society of AIME, Warrendale, PA, 1981) p. 416.

[10] A. Moslang, E. Albert, E. Recknagel, A. Weildinger and P. Moser, Hyperfine Interact. 15–16 (1983) 409.